

Atomic Manipulation of In-gap States on the β -Bi₂Pd Superconductor

Cristina Mier,^{1,*} Jiyeon Hwang,^{2,3,*} Jinkyung Kim,^{2,3} Yujeong Bae,^{2,3} Fuyuki Nabeshima,⁴ Yoshinori Imai,^{4,5} Atsutaka Maeda,⁴ Nicolás Lorente,^{1,6,†} Andreas Heinrich,^{2,3,‡} and Deung-Jang Choi^{1,6,7,§}

¹*Centro de Física de Materiales CFM/MPC (CSIC-UPV/EHU), 20018 Donostia-San Sebastián, Spain*

²*Center for Quantum Nanoscience (QNS), Institute for Basic Science (IBS), Seoul 03760, South Korea*

³*Department of Physics, Ewha Womans University, Seoul 03760, South Korea*

⁴*Department of Basic Science, University of Tokyo, Meguro, Tokyo 153-8902, Japan*

⁵*Department of Physics, Graduate School of Science, Tohoku University, Sendai, Miyagi 980-8578, Japan*

⁶*Donostia International Physics Center (DIPC), 20018 Donostia-San Sebastián, Spain*

⁷*Ikerbasque, Basque Foundation for Science, 48013 Bilbao, Spain*

(Dated: May 7, 2021)

Electronic states in the gap of a superconductor inherit intriguing many-body properties from the superconductor. Here, we create these in-gap states by manipulating Cr atomic chains on the β -Bi₂Pd superconductor. We find that the topological properties of the in-gap states can greatly vary depending on the crafted spin chain. These systems make an ideal platform for non-trivial topological phases because of the large atom-superconductor interactions and the existence of a large Rashba coupling at the Bi-terminated surface. We study two spin chains, one with atoms two-lattice-parameter apart and one with square-root-of-two lattice parameters. Of these, only the second one is in a topologically non-trivial phase, in correspondence with the spin interactions for this geometry.

PACS numbers: 74.55.+V, 74.78.-w, 74.90.+n

I. INTRODUCTION

The scanning tunneling microscope (STM) permits unprecedented control at the atomic level¹. Since the early days of STM, atoms have been moved, unveiling matter on the atomic scale^{2–6}. Atoms involve interactions that can have a profound impact on the electronic properties of host substrates, as such, designing atomic structures can lead to creating new quantum states⁷. Magnetic atoms strongly modify the low-energy electronic properties of superconductors. This is due to the appearance of *in-gap* states caused by the weakening of the Cooper-pair binding. These in-gap states are usually called Yu-Shiba-Rusinov (YSR) states^{8–10}. Recently, the interest on in-gap states has increased due to the suggestion of *topological* edge states appearing on chains of magnetic impurities on superconductors^{11–19}. These zero-energy edge states imply the presence of a topological superconducting phase. The zero-energy edge states are Majorana bound states (MBS) with non-trivial exchange transformations. Braiding of MBS is at the core of current proposals regarding topological quantum computation^{20,21}.

The STM has become a major tool in the study of MBS^{14–18,22,23}. Indeed, its spectroscopic capabilities render it unique for revealing in-gap states, granting access to unrivaled energy and space resolutions. Recently, the spatial distribution of in-gap states has been shown and used to infer new properties on the states themselves^{24–26}. The fore-mentioned STM manipulation can be used to create atomically precise spin chains on superconductors^{18,19,27}. The new in-gap states evolve into bands and open gaps displaying new forms of superconductivity^{11–13,28}. This proves the complexity of the in-

duced electronic structure. Each added impurity locally creates a few states in the superconducting gap. As the number of impurities grows, the gap *fills* up with new quasiparticle states.

The study of impurity dimers illustrates the initial steps of in-gap bands^{29–34}. The quasiparticle states themselves are difficult to describe. In the Bogoliubov-de Gennes approximation, the quasiparticle states are taken as electron and hole superpositions despite violating particle-number conservation. Furthermore, the quasiparticle states are spin polarized^{35,36}, which has important implications in the way the in-gap states hybridized²⁹. In particular, the resulting states reflect the spin-ordering of the magnetic impurities³². However, recent work suggests that in the presence of strong Rashba coupling, it is difficult to conclude on the actual spin orientation of the impurities by studying the in-gap states³³.

Here, we study atomic spin chains of Cr adsorbed on the hollow sites of β -Bi₂Pd and grown along the two main surface directions, the $\langle 100 \rangle$ and $\langle 110 \rangle$ for the Bi-terminated [001] surface using a home-built dilution fridge STM³⁷. By doing so, we are choosing two starkly different spin orientations for the chain ground state as concluded in Ref. 32. Dimers along the $\langle 100 \rangle$ -direction with a Cr-Cr distance of two-unit cells ($2a$, where a is the surface lattice parameter) present antiferromagnetic (AFM) coupling of their $5\mu_B$ magnetic moments³². Dimers along the $\langle 110 \rangle$ -direction are $\sqrt{2}a$ apart, and they are instead ferromagnetically (FM) coupled. Here, we compare dimers, trimers and tetramers of these two types of chains and conclude that the $\sqrt{2}a - \langle 110 \rangle$ chains are indeed FM coupled by comparing with model calculations of spin chains solving the Bogoliubov-de Gennes equa-

tions^{29,32}. As clearly seen in this work, the gap closes rapidly for the $\sqrt{2}a - \langle 110 \rangle$ chains, however the $2a - \langle 100 \rangle$ chains maintain an almost constant gap for chains as long as 12 Cr atoms. This has important implications for the possibility of engineering topological phases on the β -Bi₂Pd superconductor.

II. METHODS

A. Sample preparation and STM/STS characterization

The β -Bi₂Pd crystal was fabricated by the method written in Ref. 38. The chosen sample showed a T_c of 5.2 K. The Bi-terminated surface of the β -Bi₂Pd crystal was prepared by exfoliation in-situ³². Cr atoms were deposited onto a precooled β -Bi₂Pd surface at a temperature $T \leq 20$ K to have single isolated atoms. The experimental data were taken using a home-built dilution fridge STM at $T = 30$ mK and in ultra-high vacuum at the IBS Center for Quantum Nanoscience³⁷. The very-low temperature leads to a negligible thermal smearing granting a resolution higher than the one obtained by a superconducting tip³⁹⁻⁴¹. We used a metallic PtIr tip that permitted us to use the differential conductance, dI/dV , as a direct measurement of the density of states of the substrate (refer to the supplementary materials⁴² for more details). The conductance was measured using a lock-in amplifier with AC modulation bias $30 \mu V$ and frequency $330 Hz$.

Lateral atomic manipulation was achieved by approaching the STM tip to one side of a selected atom to reach junction resistances in the order of a few tens of k Ω (typically 3 mV and tens of nA). Then the STM tip was laterally moved to drag the atom to a desired position with the feedback loop open.

B. Theory

We model the Cr spin chain in the dilute spin chain limit¹³ because density-functional-theory (DFT) calculations show that no Cr d -states lie at the Fermi energy, preventing charge transfer processes³². In this framework, we solve a spin-chain using Green's functions for the superconductor in the Nambu basis set^{43,44}. We add a Rashba term to the Hamiltonian expressed in the local basis. The resulting density of states corresponds to the Bogoliubov-de Gennes states of a BCS superconductor in the presence of an array of classical spins and subject to the strong Rashba interaction of the Bi-terminated surface.

The Fermi velocity entering the superconductor's Green function^{43,44} is taken to be 0.15 (Hartree atomic units $\hbar = m = e = 1$) and the Dynes parameter⁴⁵ controlling the width of the superconducting quasiparticle peaks is 0.05 meV. This leads to peaks in the density of

states (DOS) sharper than the experimental ones, but helps the visualization of the evolution of in-gap states with the number of Cr atoms. β -Bi₂Pd is an s-wave superconductor that can be well accounted for by a single gap^{38,46} $\Delta = 0.76$ meV. For the normal metal DOS, we use $N = 0.037/eV$ that is 5 times larger than the corresponding N for a free-electron metal with Fermi velocity of 0.15 atomic units, in order to capture the 5 electrons of the Bi valence shell. The Hamiltonian taking into account the superconductor is:

$$\hat{H}_{BCS} = \xi_k \tau_0 \sigma_3 + \Delta \tau_2 \sigma_2 \quad (1)$$

Where σ_i (τ_i) are the Pauli matrices acting on the spin (particle) sectors. ξ_k is the energy from the Fermi level ($\xi_k = \epsilon_k - E_F$), the previous Hamiltonian is written in the 4-dimensional Nambu basis: $\Psi = (\hat{c}_\uparrow, \hat{c}_\downarrow, \hat{c}_\uparrow^\dagger, \hat{c}_\downarrow^\dagger)^T$.

To model the experimental system, we add the Hamiltonian describing the magnetic impurities^{43,44}. To do this, we change to a tight-binding basis, assuming a single, very-compact, atomic orbital per site. Additionally, the interactions with the magnetic impurity is assumed to be strictly localized to the site where the impurity is sitting¹³. The Hamiltonian is then:

$$\hat{H} = \hat{H}_{BCS} + \hat{H}_{impurity} = \hat{H}_{BCS} + \sum_j^N (U_j \tau_3 \sigma_0 + J_j \vec{S}_j \cdot \vec{\alpha}) \quad (2)$$

with $\vec{\alpha} = \frac{1+\tau_3}{2} \vec{\sigma} + \frac{1-\tau_3}{2} \sigma_2 \vec{\sigma} \sigma_2$, where $\vec{\sigma}$ is the spin operator⁹. This Hamiltonian describes a BCS superconductor and the interaction between its electrons and N extra impurities. The interaction contains an exchange coupling, with strength J_j , and a non-magnetic potential scattering term, U_j , per impurity j . We will use the same impurity species, Cr, and assume that they are equivalent regardless of their adsorption site and spin chain, in order to study the system's evolution with the number of atoms in the spin chains. And $\vec{S}_j = (S_{j,x}, S_{j,y}, S_{j,z}) = S(\sin \theta_j \cos \phi_j, \sin \theta_j \sin \phi_j, \cos \theta_j)$ is the spin of atom j considered to be a classical spin and hence not an operator. The local term U_j describes a scalar potential acting on the substrate's electron. It is responsible for the potential scattering term produced by the impurity. In the case of a charged impurity, U_j is mainly given by the Coulomb interaction between the total charge of the impurity and the charge of the substrate's electron. The potential scattering that explains the electron-hole asymmetry of the YSR bands is taken as $U_j = 5.5$ eV. The values for the Kondo-exchange coupling, J_j , are about 2 eV as estimated from fittings to a single-Cr YSR states³².

The Hamiltonian is completed by a Rashba term:

$$\begin{aligned} \hat{H}_{Rashba} = & i \frac{\alpha_R}{2a} \sum_{i,j,\alpha,\beta} [\hat{c}_{i+1,j,\alpha}^\dagger (\sigma_2)_{\alpha,\beta} \hat{c}_{i,j,\beta} \\ & - \hat{c}_{i,j+1,\alpha}^\dagger (\sigma_1)_{\alpha,\beta} \hat{c}_{i,j,\beta} + h.c.] \quad (3) \end{aligned}$$

where α, β are spin indexes. The interaction couples spins on nearest-neighbour sites. The lattice parameter of the

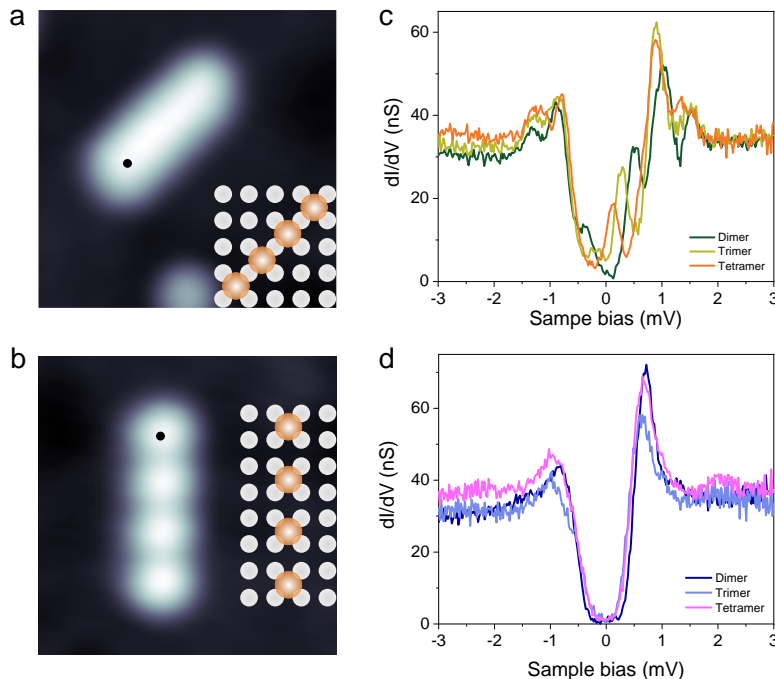


FIG. 1. Chromium chains built on β -Bi₂Pd surface by atomic manipulation. Topographic images of (a) $\sqrt{2}a - \langle 110 \rangle$ and (b) $2a - \langle 100 \rangle$ unit-cell apart tetramer chains (100 mV, 10 pA, $4 \times 4 \text{ nm}^2$). The insets show the atomic geometry of the tetramer nanostructures. The corresponding differential conductance is measured at the end atom (marked black dot) from dimer, trimer to tetramer in (c) $\sqrt{2}$ unit-cell apart and (d) 2 unit-cell apart tetramer chains. ($T = 30 \text{ mK}$, AC modulation bias $30 \mu\text{V}$)

substrate is a , and the factor of $2a$ comes from a finite-difference scheme to obtain the above discretized version of the Rashba interaction. For the case of Bi₂Pd, we use a large Rashba coupling, $\alpha_R \approx 1.8 \text{ eV} \cdot \text{\AA}$ as coming from our DFT calculations and in agreement with the couplings of Bi-terminated surfaces⁴⁷.

The local or projected DOS (PDOS) is computed over every local orbital i of the basis using,

$$\rho(i, \omega) = -\frac{1}{\pi} \text{Im}[G_{i,i}^{1,1}(\omega) + G_{i,i}^{4,4}(-\omega)] \quad (4)$$

Where $G_{ii}^{\nu,\mu}$ is the resulting Green's function evaluated on orbital i for the Nambu components ν and μ by solving Dyson's equation:

$$\hat{G} = [\hat{G}_{BCS}^{-1} - \hat{H}_I]^{-1} \quad (5)$$

Where \hat{G}_{BCS} is the retarded Green's operator for the BCS Hamiltonian from Eq.(1) and $\hat{H}_I = \hat{H}_{impurity} + \hat{H}_{Rashba}$.

The DFT calculations were performed using the VASP code⁴⁸. The β -Bi₂Pd slab was optimized using the Perdew-Burke-Ernzerhof (PBE) form of the generalised gradient approximation (GGA)⁴⁹, following the calculations of Ref. 32. For more details, please see the supplementary materials⁴².

III. RESULTS AND DISCUSSION

The dI/dV over a single Cr adatom yields a single YSR state given by peaks at $V = \pm 0.35 \text{ mV}$ (please see Refs. 32 and 42). By lateral atomic manipulation, we place Cr atoms to create linear $\sqrt{2}a - \langle 110 \rangle$ or $2a - \langle 100 \rangle$ chains. Figure 1 (a) and (b) show constant-current images of the two tetramer chains. The (a) chain corresponds to the $\sqrt{2}a - \langle 110 \rangle$ tetramer as depicted in the inset, the (b) is the $2a - \langle 100 \rangle$ tetramer. As the chain is made larger, misplacing a Cr atom becomes more common. Indeed, error-free $\sqrt{2}a - \langle 110 \rangle$ spaced nanostructures were difficult to obtain, while $2a - \langle 100 \rangle$ chains are easier to manipulate. The reason lies in the chemistry of the chains. For the more compact chains, the affinity of Cr atoms for certain conformations leads to non-linear arrangements. The less compact $2a - \langle 100 \rangle$ chain is easier to fabricate by single-atom manipulation because the atoms do not approach each other as much and hence cluster formation is much less common.

Our DFT calculations yield a coherent picture with the experiment. The Cr atoms are preferentially adsorbed on the hollow sites of the Bi-riched surface³², and the Cr-Cr interactions in the chains are mediated by a single Bi atom in the $\sqrt{2}a - \langle 110 \rangle$ chains or a square of four Bi atoms in the $2a - \langle 100 \rangle$ chains. Short $1a - \langle 100 \rangle$ chains can also be obtained, but the structures easily become clusters due to the Cr-Cr interaction. The $\sqrt{2}a - \langle 110 \rangle$

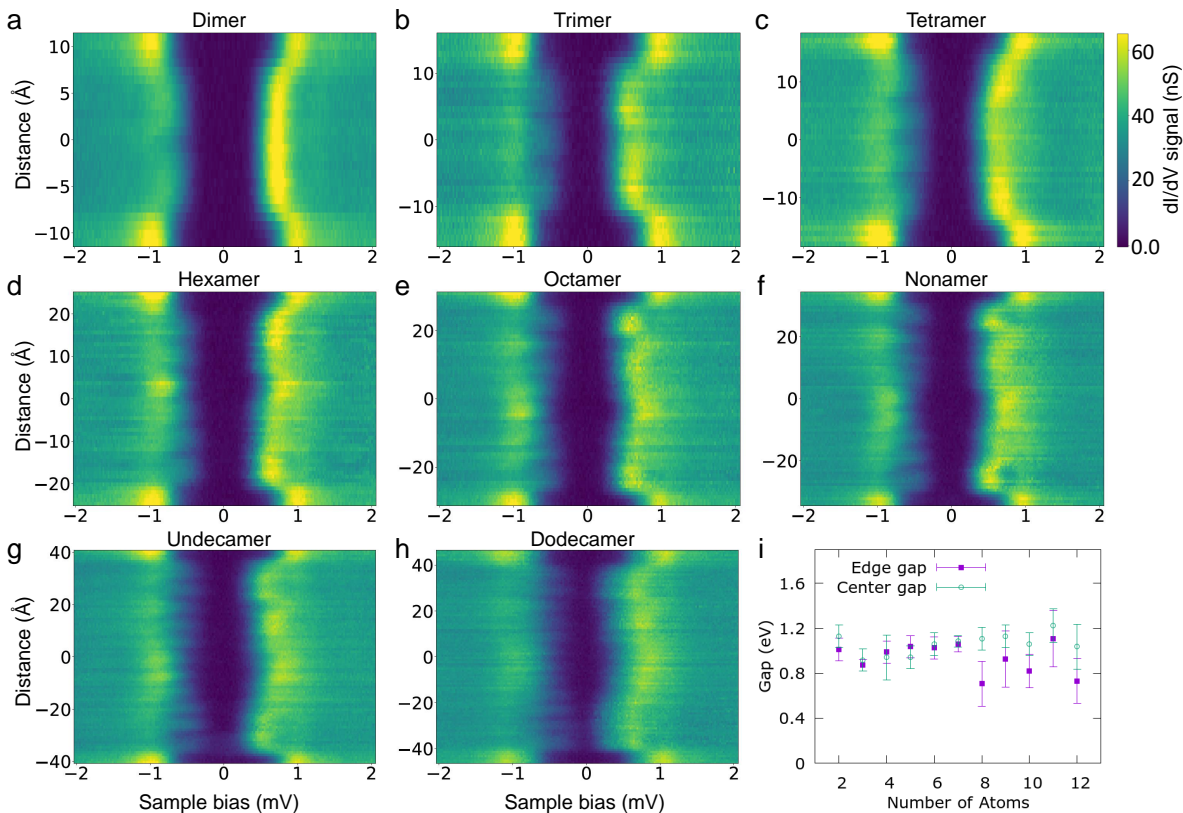


FIG. 2. Differential conductance measured along $\text{Cr}_n 2a - \langle 100 \rangle$ chains with $n = 2$ in (a), $n = 3$ in (b), $n = 4$ in (c), $n = 6$ in (d), $n = 8$ in (e), $n = 9$ in (f), $n = 11$ in (g), $n = 12$ in (h). The x -axis represents the sample bias, the y -axis displays the distances over the chain. The color code gives the intensity of the differential conductance. The smallest gap in the system, defined as the distance between the lower quasiparticle peak and the highest quasihole peak is plotted in (i). In the absence of Cr atoms, the gap corresponds to 2Δ where $\Delta = 0.75$ meV for Bi_2Pd . The gap has been obtained at an edge atom or at the center of the spin chain.

dimer is 249 meV less stable than the $1a - \langle 100 \rangle$ dimer. As a consequence, shifting a single Cr atom towards another Cr to reach the short $\sqrt{2}a$ distance likely produces a $1a - \langle 100 \rangle$ dimer. This stacking error becomes more likely as the chain is manipulated more times to make it longer. The $2a - \langle 100 \rangle$ dimer is only 30 meV less stable than the $\sqrt{2}a - \langle 110 \rangle$. But, still the interactions between atoms for the larger Cr-Cr distance, $2a - \langle 100 \rangle$ chains, are weaker resulting in an easier manipulation to build longer chains. Indeed, the bottom-up approach of chain building is difficult on many other substrates⁵⁰. Recent experiments show long Mn chains built in a similarly compact geometry as here but on a Nb(110) substrate, also giving rise to topological in-gap behavior^{51,52}.

Once the chains are built, the differential conductance, dI/dV , as a function of bias, V , and surface position, is an extraordinary probe of the electronic properties of the new systems. Figure 1 (c) and (d) shows dI/dV spectra measured at $T = 30$ mK for the dimer, trimer and tetramer of $\sqrt{2}a - \langle 110 \rangle$ and $2a - \langle 100 \rangle$ type, respectively. The dI/dV spectra are taken at an edge atom (black dot in Fig. 1 (a) and (b)). The two sets (c) and (d) are

starkly in contrast. Figure 1 (c) clearly shows an in-gap state that is shifting towards zero bias as the chain gets longer. With opposite behavior, Fig. 1 (d) shows no clear in-gap state and a well-formed gap. Furthermore, the gap for the dimer is larger but the trimer and tetramer show similar gaps, pointing at a rapid stabilization of gap with chain size.

The in-gap states of the $\sqrt{2}a - \langle 110 \rangle$ dimer agree well with a model of two FM aligned spins and they disappear if the magnetic moments are coupled AFM as in Fig. 1 (d) for a $2a - \langle 100 \rangle$ dimer³². The $2a - \langle 100 \rangle$ -dimer behavior can be justified by the mutual cancellation of both spins, although the actual explanation is more involved. This can be seen by studying the spatial distribution of the differential conductance along the two types of chains. Figure 2 and 3 show the dI/dV in a color code (bright-yellow corresponds to larger conductance and dark-blue represents zero conductance) along the chain, y -axis in Å of the distances over the chain, and x -axis in mV of the STM junction's bias.

Figure 2 shows the results for the $2a - \{100\}$ spin chains. As seen in Fig. 1 (d), we find no obvious struc-

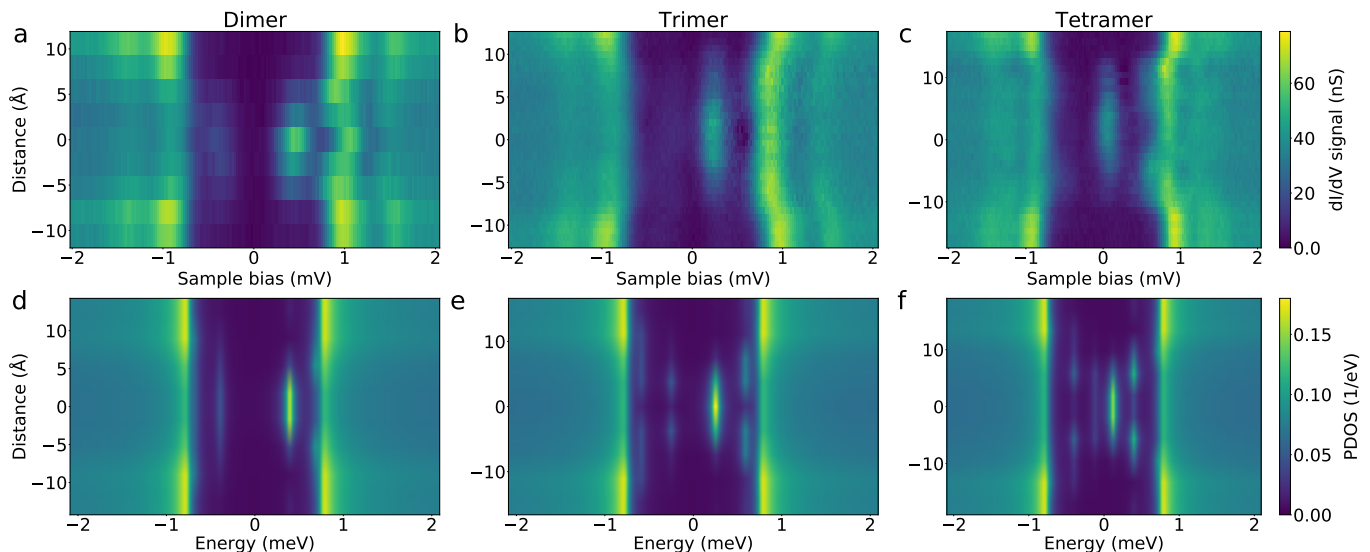


FIG. 3. Experimental differential conductance measured along the Cr adatoms of the $\sqrt{2}a - \langle 110 \rangle$ (a) dimer, (b) trimer and (c) tetramer chains. The corresponding calculations for ferromagnetically coupled $\sqrt{2}a - \langle 110 \rangle$ (d) dimer, (e) trimer and (f) tetramer chains are depicted in the lower row. The color code refers to the projected density of states (PDOS) on the different sites of the tight-binding lattice, in this case the one corresponding to the Cr adatoms.

ture in the gap in any of the studied chains. A closer look reveals atomic modulations of the quasiparticle states that match the number of atoms in the chains. The presence of YSR states can be inferred by the profile of the gap. The complete sequence of chains from $n = 2$ to $n = 12$ can be found in the supplemental material⁴². All chains roughly show a smaller gap at the edge atoms than at the center of the chain, see Fig. 2 (i). In first approximation, the gap is constant with chain length. Beyond 8 atoms, the chains show a smaller gap at the edge. However, the closing of the gap is very small and almost constant for longer chains. These data indicate that the YSR states are not able to close the superconducting gap, preventing any topological phase transition.

Figure 3 presents the dI/dV maps of the $\sqrt{2}a - \langle 110 \rangle$ chains (upper row) compared to model calculations of the PDOS on the surface sites (lower row). Figure 3 shows excellent agreement between experiment and theory if the magnetic moments are FM coupled, which is also in good agreement with the results of Ref. 32. The calculations of the YSR structure confirm the FM ordering for Cr atoms sitting along the $\sqrt{2}a - \langle 110 \rangle$ hollow sites. Moreover, the magnetic ordering is not altered by adding extra atoms to the dimer.

The data of Fig. 3 permit us to have a clear picture of the in-gap states for the $\sqrt{2}a - \langle 110 \rangle$ chains. The dimer presents two YSR bands, one closer to zero energy with a larger density of states between the two Cr adatoms, and one closer to the quasiparticle continuum with a minimum between the atoms. Adding one more atom to form the trimer shifts the lowest-energy YSR state closer to zero, but keeps its overall spatial distribution with a maximum PDOS on the central atom. Furthermore, we

find the second band closer to the quasiparticle continuum, and again with a minimum of PDOS over the central point of the chain. We also notice that as in the dimer case, the quasiparticle PDOS presents a reduction and an oscillation along the chain. Finally, the tetramer shifts both bands closer to zero, but largely keeping their spatial distributions. The PDOS at the quasiparticle edge presents the same features as for the dimer and trimer.

In order to match the very fast experimental closing of the gap with the chain length, the Kondo exchange coupling (J) is increased from $J = 2.0$ eV for the dimer, $J = 2.1$ eV for the trimer, and $J = 2.3$ eV for the tetramer, respectively in Fig. 3 (d), (e) and (f). This behavior can be rationalized by a possible geometrical and electronic rearrangement of the chain as the spin chain grows in size. The atoms place themselves more symmetrically and closer to the surface leading to a larger hybridization with the substrate and thus to larger couplings.

The MBS appear naturally as soon as the exchange coupling J is larger than 2.3 eV. It is interesting to study how the appearance of MBS takes place as J varies. This is plotted in Fig. 4. The pannels are arranged in three columns. Each column corresponds to a different value of J . The first one is $J = 2.1$ eV, the second one $J = 2.3$ eV and the fourth one is $J = 2.5$ eV. The first row plots the PDOS along the chain (y -axis) as a function of the quasiparticle energy (x -axis). We see the formation of YSR bands already for this 20-atom chain. In the middle of the chain, there is a clear gap in the YSR structure. For small J , this gap is maintained all along the chain, for the larger J , the gap is closed by an edge state that is a MBS as we shall briefly see. For $J = 2.3$ eV, we

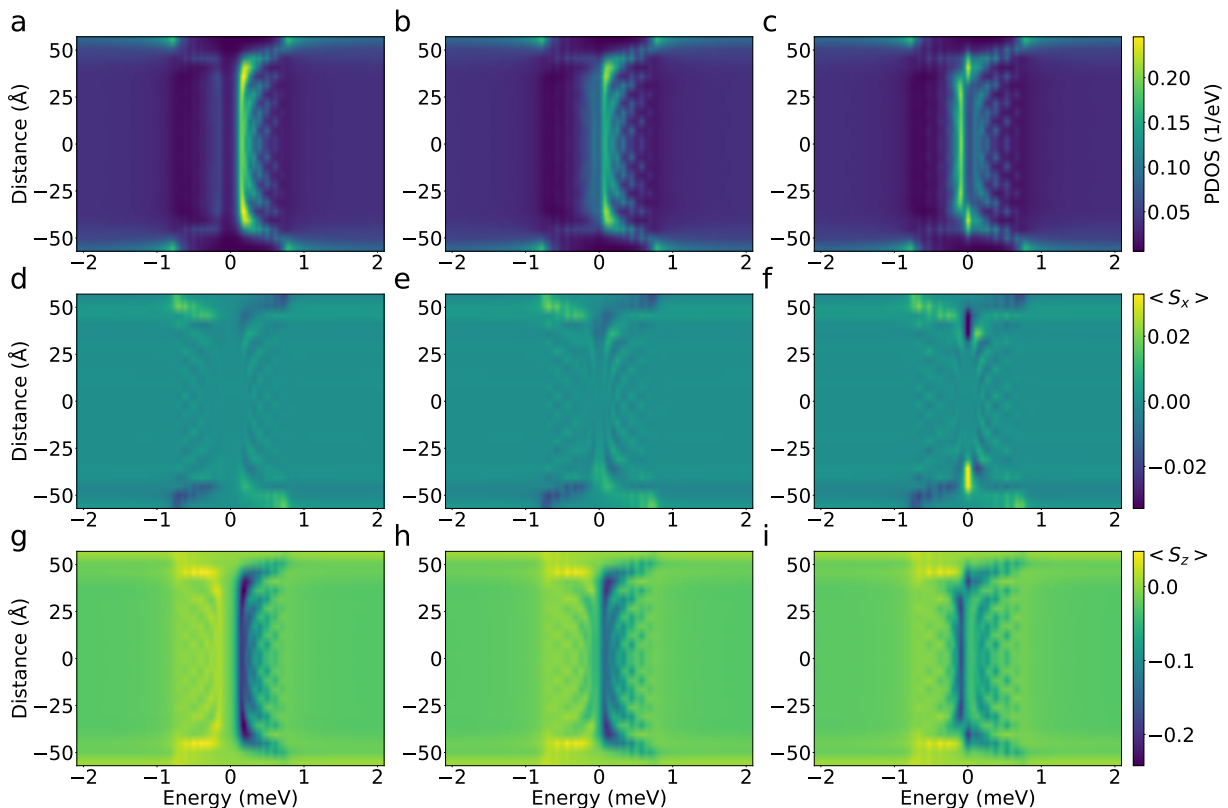


FIG. 4. Topological phase transition induced by increasing the exchange coupling J . The three rows of panels of this figure correspond to three different values of the exchange coupling (a) $J = 2.1$ eV, (b) $J = 2.3$ eV and (c) $J = 2.5$ eV for the PDOS showing the quasiparticle states induced by a $\text{Cr}_{20} \sqrt{2}a - \langle 110 \rangle$ chain. We see that the gap is virtually closed for (b) $J = 2.3$ eV and reopens for (c) $J = 2.5$ eV displaying the MBS that indicates the change of topological phase of the superconductor. Panels (d), (e), (f) correspond to the respective values of J and show the transversal spin density $\langle S_x \rangle$ along the chain. We see that $\langle S_x \rangle$ only becomes large and of opposite sign at the two MBS. Finally, panels (g), (h), (i) show the spin density, $\langle S_z \rangle$, of the YSR states for the three different couplings. We find that the spin across the gap reverts when the TPT is achieved and the corresponding MBS have the same well defined spin.

see that the lowest-energy bands are still separated by a very small gap, almost closing and for $J = 2.5$ the gap is well-formed again. The closing and reopening of the gap is a necessary condition to change to a topologically non-trivial superconducting band structure.

The second row is the transversal spin density component $\langle S_x \rangle$ along the chain for the same YSR state as above. We see that the values are small and dispersed for $J = 2.1$ and 2.3 eV. For $J = 2.3$ eV the values of $\langle S_x \rangle$ extend all over the superconducting gap giving the impression of many YSR states closing the gap. But $J = 2.5$ eV is very different. The gap in $\langle S_x \rangle$ is again clear and very sharp values at just the edge states appear and are of opposite sign. This is a clear signature of a MBS⁵³.

The third row shows the spin of the YSR states. From the above data, we have evidence that a topological phase transition (TPT) has taken place between $J = 2.1$ eV and $J = 2.5$ eV, $J = 2.3$ eV being near to the closing of the gap. The spin shows it unambiguously. The YSR bands show opposite spin polarizations for their particle and hole components. This is clearly seen across the YSR gap. But the character has changed between $J = 2.1$ eV

and $J = 2.5$ eV because the spin polarization is the opposite one. This is a clear hallmark of a TPT⁵⁴. The edge states show the same spin polarization as corresponds to the MBS⁵³.

The experimental data show that the gap is almost closed for the tetramer $\text{Cr}_4 \sqrt{2}a - \langle 110 \rangle$ spin chain. Closing the gap is a necessary condition for a topological phase transition (TPT). Figure 4 clearly show that the edge states for J larger than 2.3 eV are indeed MBS, and that the TPT takes place somewhere close to 2.3 eV. The change of YSR band character through the TPT is clearly seen in the YSR spin polarization⁵⁴, indeed the spin inverts across the transition.

Figure 5 shows the calculation of a $\text{Cr}_{20} \sqrt{2}a - \langle 110 \rangle$ spin chain with $J = 2.5$ eV. A clear spin-polarized edge state appears, with opposite transversal spin components ($\langle S_x \rangle$) on the chain edges showing that indeed MBS are formed⁵³. The number of atoms in the spin chain is decisive to clearly show MBS. However, short chains may suffice to prove that indeed the superconductor undergoes a TPT.

For a spin chain in the topological phase, the appear-

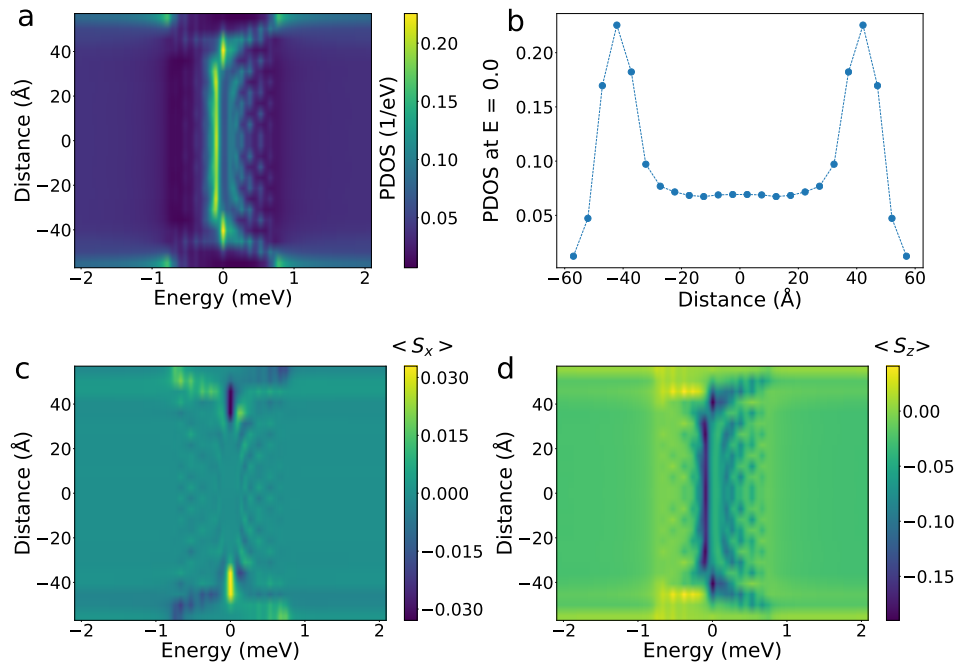


FIG. 5. Majorana bound states in a 20-atom $\sqrt{2}a - \langle 110 \rangle$ Cr spin chain. (a) Color map plotting the PDOS as a function of energy and distance. There is a clear state localized at the edges of the chain and at exactly zero energy. (b) PDOS along the 20-Cr chain, x -axis are distances in Å along the Cr chain. The localization of the PDOS to the edges at zero energy spans the four Cr edge atoms, and the PDOS sharply fall beyond. The value of the PDOS between edges reduces as the chain length increases. (c) Color map (dark: negative, light: positive) showing that the transversal spin density, $\langle S_x \rangle$, changes sign with edge, but (d) the out of plane spin-density component, $\langle S_z \rangle$, is the same for both edges. Moreover, these data can be correlated with a clear change of spin sign across the gap as the exchange-interaction value, J , is increased that shows the closing and reopening of the gap into the topological phase. All these data signal the presence of a Majorana bound state in a 20-atom $\sqrt{2}a - \langle 110 \rangle$ Cr spin chain.

ance of the MBS needs a certain minimum chain size. This is because the MBS have a certain extension and they overlap for small chains. The consequence is that the zero-energy state becomes localized in the center of the chain, and it is difficult to identify the new superconducting phase as topological.

The behavior of MBS with the chain's length is shown in Fig. 6 for $Cr_n \sqrt{2}a - \langle 110 \rangle$ chains with n from 5 to 20. The parameters are the above ones with $J = 2.5$ eV that correspond to the topological phase. In the case of the pentamer, Fig. 6 (a) clearly shows a closed gap. We find a zero-energy state for Cr_5 that looks very similar to the experimental (and theoretical) one for Cr_4 . The zero-energy state is clearly localized in the center of the chain. As the chain length is increased, the state localizes to the edges. At the same time there is an excitation gap appearing in the center of the chain. For $n = 8$ atoms, it is already possible to clearly differentiate the features of the well-formed MBS even though the chain is still small and the YSR states present a strong discrete nature. As the length is increased, a clear MBS appears. These calculations imply that $Cr_n \sqrt{2}a - \langle 110 \rangle$ chains on β -Bi₂Pd will clearly show MBS and topological features at fairly small chains. Indeed, 20 atoms suffice to have an unambiguous topological spin chain.

IV. CONCLUSION

In summary, $Cr_n \sqrt{2}a - \langle 110 \rangle$ spin chains on β -Bi₂Pd show a fast closing of the superconducting gap as the number of atoms in the chain increases. As few as four Cr atoms suffice to have in-gap states closing down the gap. We show that an 8-atom $\sqrt{2}a - \langle 110 \rangle$ chain may already display all features of MBS. Our study reveals that the $\sqrt{2}a - \langle 110 \rangle$ Cr spin chain shows ferromagnetic alignment of its spins. The large magnetic moment of Cr plus a sizable Rashba coupling of the β -Bi₂Pd surface leads to the topological phase transition. Increasing the distance between Cr atoms leads to facile atom manipulation that translates in longer chains of Cr atoms on β -Bi₂Pd but at the cost of not reaching a topological phase. Indeed, our measurements show a persistent gap rather constant with chain length for $Cr_n 2a - \langle 100 \rangle$, showing that this type of chains will not induce a topological phase transition on the β -Bi₂Pd superconductor.

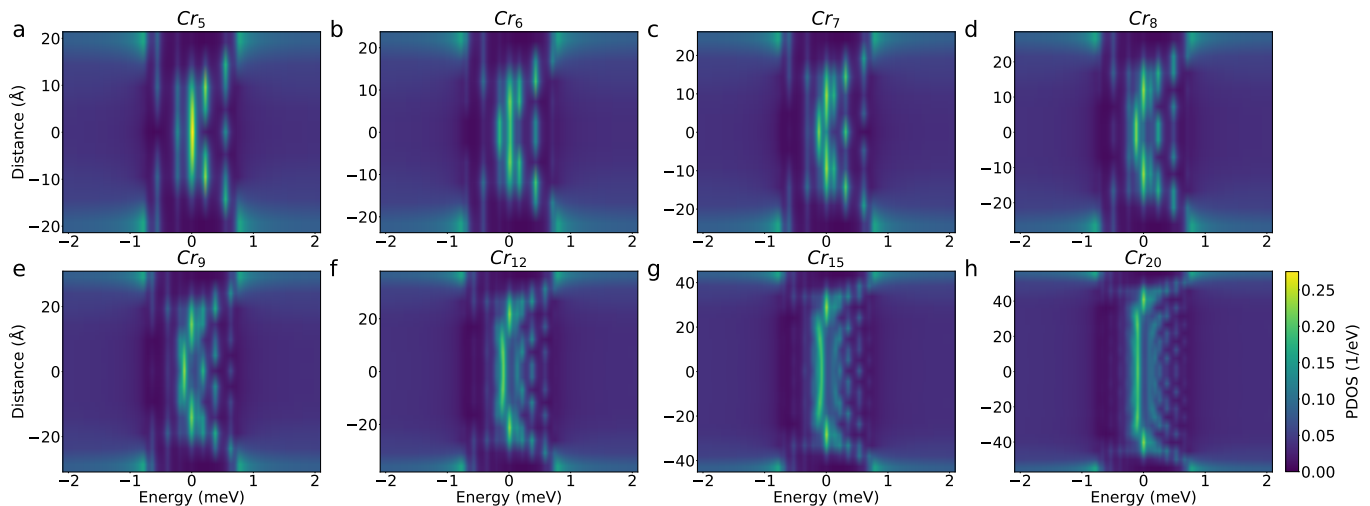


FIG. 6. $Cr_n \sqrt{2}a - \langle 110 \rangle$ chains with n from 5 to 20, for $J = 2.5$ eV such that the superconductor is in the topological phase. The zero-energy state moves away from the center of the chain to the borders as the chain is increased in size. At fairly low numbers, 8 or even 7 atoms, the MBS become clear and a gap is formed at the center of the chain.

ACKNOWLEDGEMENT

Financial support from the Spanish MICINN (projects RTI2018-097895-B-C44 and Excelencia EUR2020-

112116), Eusko Jaurlaritza (project PIBA_2020_1.0017), JSPS KAKENHI (JP18K03531 and JP19K14651), and the Institute for Basic Science (grant IBS-R027-D1) is gratefully acknowledged.

* These authors contributed equally

† nicolas.lorente@ehu.eus

‡ heinrich.andreas@qns.science

§ djchoi@dipc.org

¹ P. Avouris, *Accounts of Chemical Research* **28**, 95 (1995), publisher: American Chemical Society.

² D. M. Eigler and E. K. Schweizer, *Nature* **344**, 524 (1990).

³ J. A. Stroscio and D. M. Eigler, *Science* **254**, 1319 (1991), publisher: American Association for the Advancement of Science Section: Articles.

⁴ G. Meyer, S. Zöphel, and K. H. Rieder, *Applied Physics A* **63**, 557 (1996).

⁵ K. Morgenstern, N. Lorente, and K.-H. Rieder, *physica status solidi (b)* **250**, n/a (2013).

⁶ S. Clair and D. G. de Oteyza, *Chemical Reviews* **119**, 4717 (2019), publisher: American Chemical Society.

⁷ A. A. Khajetoorians, D. Wegner, A. F. Otte, and I. Swart, *Nature Reviews Physics* **1**, 703 (2019), number: 12 Publisher: Nature Publishing Group.

⁸ L. Yu, *Acta Physica Sinica* **21**, 75 (1965).

⁹ H. Shiba, *Progress of Theoretical Physics* **40**, 435 (1968).

¹⁰ A. I. Rusinov, *Soviet Journal of Experimental and Theoretical Physics* **9**, 85 (1969).

¹¹ T.-P. Choy, J. M. Edge, A. R. Akhmerov, and C. W. J. Beenakker, *Physical Review B* **84**, 195442 (2011).

¹² S. Nadj-Perge, I. K. Drozdov, B. A. Bernevig, and A. Yazdani, *Phys. Rev. B* **88**, 020407 (2013).

¹³ F. Pientka, L. I. Glazman, and F. von Oppen, *Physical Review B* **88**, 155420 (2013).

¹⁴ S. Nadj-Perge *et al.*, *Science* **346**, 602 (2014).

¹⁵ M. Ruby *et al.*, *Phys. Rev. Lett.* **115**, 197204 (2015).

¹⁶ R. Pawlak, M. Kisiel, J. Klinovaja, T. Meier, S. Kawai, T. Glatzel, D. Loss, and E. Meyer, *Npj Quantum Information* **2**, 16035 (2016).

¹⁷ S. Nadj-Perge, I. K. Drozdov, J. Li, H. Chen, S. Jeon, J. Seo, A. H. MacDonald, B. A. Bernevig, and A. Yazdani, *Science*, 1259327 (2014).

¹⁸ H. Kim, A. Palacio-Morales, T. Posske, L. Rózsa, K. Palotás, L. Szunyogh, M. Thorwart, and R. Wiesendanger, *Science Advances* **4**, eaar5251 (2018).

¹⁹ D.-J. Choi, N. Lorente, J. Wiebe, K. von Bergmann, A. F. Otte, and A. J. Heinrich, *Reviews of Modern Physics* **91**, 041001 (2019), publisher: American Physical Society.

²⁰ A. Kitaev, *Annals of Physics* **303**, 2 (2003).

²¹ C. Nayak, S. H. Simon, A. Stern, M. Freedman, and S. Das Sarma, *Rev. Mod. Phys.* **80**, 1083 (2008).

²² A. Palacio-Morales, E. Mascot, S. Cocklin, H. Kim, S. Rachel, D. K. Morr, and R. Wiesendanger, *Science Advances* **5** (2019), 10.1126/sciadv.aav6600.

²³ B. Jäck, Y. Xie, and A. Yazdani, “Detecting and distinguishing majorana zero modes with the scanning tunneling microscope,” (2021), arXiv:2103.13210 [cond-mat.mes-hall].

²⁴ G. C. Ménard, S. Guissart, C. Brun, S. Pons, V. S. Stolyarov, F. Debontridder, M. V. Leclerc, E. Janod, L. Cario, D. Roditchev, P. Simon, and T. Cren, *Nature Physics* **11**, 1013 (2015).

²⁵ M. Ruby, *et al.*, *Phys. Rev. Lett.* **117**, 186801 (2016).

²⁶ D.-J. Choi, C. Rubio-Verdú, J. de Bruijckere, M. M. Ugeda, N. Lorente, and J. I. Pascual, *Nature Communications* **8**, 15175 (2017).

- ²⁷ A. Kamlapure, L. Cornils, J. Wiebe, and R. Wiesendanger, *Nature Communications* **9**, 3253 (2018).
- ²⁸ Y. Peng, F. Pientka, L. I. Glazman, and F. von Oppen, *Phys. Rev. Lett.* **114**, 106801 (2015).
- ²⁹ M. E. Flatté and D. E. Reynolds, *Phys. Rev. B* **61**, 14810 (2000).
- ³⁰ S. Kezilebieke, M. Dvorak, T. Ojanen, and P. Liljeroth, *Nano Letters* **18**, 2311 (2018), publisher: American Chemical Society.
- ³¹ M. Ruby, B. W. Heinrich, Y. Peng, F. von Oppen, and K. J. Franke, *Phys. Rev. Lett.* **120**, 156803 (2018).
- ³² D.-J. Choi, C. G. Fernández, E. Herrera, C. Rubio-Verdú, M. M. Ugeda, I. Guillamón, H. Suderow, J. I. Pascual, and N. Lorente, *Phys. Rev. Lett.* **120**, 167001 (2018).
- ³³ P. Beck, L. Schneider, L. Rózsa, K. Palotás, A. Lászlóffy, L. Szunyogh, J. Wiebe, and R. Wiesendanger, arXiv:2010.04031 [cond-mat] (2020), arXiv: 2010.04031.
- ³⁴ H. Ding, Y. Hu, M. T. Randeria, S. Hoffman, O. Deb, J. Klinovaja, D. Loss, and A. Yazdani, *Proceedings of the National Academy of Sciences* **118** (2021), 10.1073/pnas.2024837118, <https://www.pnas.org/content/118/14/e2024837118.full.pdf>.
- ³⁵ L. Cornils, A. Kamlapure, L. Zhou, S. Pradhan, A. Khajetoorians, J. Fransson, J. Wiebe, and R. Wiesendanger, *Physical Review Letters* **119**, 197002 (2017).
- ³⁶ L. Schneider, P. Beck, J. Wiebe, and R. Wiesendanger, *Science Advances* **7**, eabd7302 (2021), publisher: American Association for the Advancement of Science Section: Research Article.
- ³⁷ J. Kim, W.-J. Jang, T. H. Bui, D.-J. Choi, C. Wolf, F. Delgado, D. Krylov, S. Lee, S. Yoon, C. P. Lutz, A. J. Heinrich, and Y. Bae, “Spin resonance amplitude and frequency of a single atom on a surface in a vector magnetic field,” (2021), arXiv:2103.09582 [cond-mat.mes-hall].
- ³⁸ Y. Imai, F. Nabeshima, T. Yoshinaka, K. Miyatani, R. Kondo, S. Komiyama, I. Tsukada, and A. Maeda, *Journal of the Physical Society of Japan* **81**, 113708 (2012).
- ³⁹ J. G. Rodrigo, H. Suderow, S. Vieira, E. Bascones, and F. Guinea, *Journal of Physics: Condensed Matter* **16**, R1151 (2004).
- ⁴⁰ S.-H. Ji, T. Zhang, Y.-S. Fu, X. Chen, X.-C. Ma, J. Li, W.-H. Duan, J.-F. Jia, and Q.-K. Xue, *Phys. Rev. Lett.* **100**, 226801 (2008).
- ⁴¹ C. Mier, B. Verlhac, L. Garnier, R. Robles, L. Limot, N. Lorente, and D.-J. Choi, *The Journal of Physical Chemistry Letters* **12**, 2983 (2021), <https://doi.org/10.1021/acs.jpcllett.1c00328>.
- ⁴² Please refer to the Supplemental Material.
- ⁴³ M. E. Flatté, *Phys. Rev. B* **61**, R14920 (2000).
- ⁴⁴ M. E. Flatté and J. M. Byers, *Phys. Rev. Lett.* **78**, 3761 (1997).
- ⁴⁵ R. C. Dynes, V. Narayanamurti, and J. P. Garno, *Phys. Rev. Lett.* **41**, 1509 (1978).
- ⁴⁶ E. Herrera, I. Guillamón, J. A. Galvis, A. Correa, A. Fente, R. F. Luccas, F. J. Mompean, M. Garcia-Hernandez, S. Vieira, J. P. Brison, and H. Suderow, *Physical Review B* **92**, 054507 (2015).
- ⁴⁷ S. V. Ereemeev, I. P. Rusinov, I. A. Nechaev, and E. V. Chulkov, *New Journal of Physics* **15**, 075015 (2013).
- ⁴⁸ G. Kresse and J. Furthmüller, *Computational Materials Science* **6**, 15 (1996).
- ⁴⁹ J. P. Perdew, K. Burke, and M. Ernzerhof, *Physical Review Letters* **77**, 3865 (1996).
- ⁵⁰ M. Steinbrecher, R. Rausch, K. T. That, J. Hermenau, A. A. Khajetoorians, M. Potthoff, R. Wiesendanger, and J. Wiebe, *Nature Communications* **9**, 2853 (2018).
- ⁵¹ L. Schneider, P. Beck, T. Posske, D. Crawford, E. Mascot, S. Rachel, R. Wiesendanger, and J. Wiebe, arXiv:2104.11497 [cond-mat] (2021), arXiv: 2104.11497.
- ⁵² L. Schneider, P. Beck, J. Neuhaus-Steinmetz, T. Posske, J. Wiebe, and R. Wiesendanger, arXiv:2104.11503 [cond-mat] (2021), arXiv: 2104.11503.
- ⁵³ D. Sticlet, C. Bena, and P. Simon, *Phys. Rev. Lett.* **108**, 096802 (2012).
- ⁵⁴ M. Mashkooori, S. Pradhan, K. Björnson, J. Fransson, and A. M. Black-Schaffer, *Phys. Rev. B* **102**, 104501 (2020).

Supplementary Material for: Atomic Manipulation of In-gap States on the β -Bi₂Pd Superconductor

Cristina Mier,^{1,*} Jiyeon Hwang,^{2,3,*} Jinkyung Kim,^{2,3} Yujeong Bae,^{2,3} Fuyuki Nabeshima,⁴ Yoshinori Imai,^{4,5} Atsutaka Maeda,⁴ Nicolás Lorente,^{1,6,†} Andreas Heinrich,^{2,3,‡} and Deung-Jang Choi^{1,6,7,§}

¹*Centro de Física de Materiales CFM/MPC (CSIC-UPV/EHU), 20018 Donostia-San Sebastián, Spain*

²*Center for Quantum Nanoscience (QNS), Institute for Basic Science (IBS), Seoul 03760, South Korea*

³*Department of Physics, Ewha Womans University, Seoul 03760, South Korea*

⁴*Department of Basic Science, University of Tokyo, Meguro, Tokyo 153-8902, Japan*

⁵*Department of Physics, Graduate School of Science, Tohoku University, Sendai, Miyagi 980-8578, Japan*

⁶*Donostia International Physics Center (DIPC), 20018 Donostia-San Sebastián, Spain*

⁷*Ikerbasque, Basque Foundation for Science, 48013 Bilbao, Spain*

(Dated: May 7, 2021)

COMPARISON OF THE dI/dV SPECTRA USING METALLIC AND SUPERCONDUCTING TIPS

We used a dilution fridge STM operating at $T = 30$ mK [1]. The benefit of measuring at a very-low temperature leads to a negligible thermal smearing granting a higher energy resolution in a range of a few tens of μeV . Measuring with a superconducting tip increases the energy resolution due to the sharp quasi-particle peaks at the tip side [2] but afterward, a deconvolution process is required to get the density of states of the sample [3, 4]. Figure 1 shows the comparison of the dI/dV spectra measured using a superconducting tip at 1.2 K and a non-superconducting metallic tip at 30 mK. We use a metallic PtIr tip that permitted us to use the dI/dV as a direct measurement of the density of states of the substrate without any deconvolution process.

LOCAL SPECTRA OF THE $\text{Cr}_n 2a - \langle 100 \rangle$ SPIN CHAINS

Figure 2 shows all the spectra obtained along the spin chains formed by $\text{Cr}_n 2a - \langle 100 \rangle$ on β -Bi₂Pd with $n = 2, \dots, 12$. The evolution is very smooth and the features are very similar. Namely, the in-gap states are very close to the superconductor's quasiparticle peaks, and a clear, almost constant gap is maintained. Beyond $n = 8$, the gap measured at the edge slightly closes down, and an excited-state edge state starts developing. However, as far as $n = 12$ the gap at the edge stays constant and there is no indication of any gap closing for $\text{Cr}_n 2a - \langle 100 \rangle$ on Bi₂Pd. The gap has been evaluated by taking the distance between peaks in the second derivative, d^2I/dV^2 , after a 5-point smoothing of the experimental data.

DENSITY FUNCTIONAL THEORY CALCULATIONS

The DFT calculations were performed using the VASP code [5]. The calculations performed here extend the ones in Ref. [6]. The β -Bi₂Pd slab was optimized using the Perdew-Burke-Ernzerhof (PBE) form of the generalised gradient approximation (GGA) [7], obtaining a bulk lattice parameter $a = b = 3.406 \text{ \AA}$ and $c = 13.011 \text{ \AA}$ in good agreement with other DFT calculations and the experimental value of $3.36(8) \text{ \AA}$ and $12.97(2) \text{ \AA}$ given in Ref. [8]. The surface calculations were performed for Bi-terminated slabs with four Bi layers and two Pd ones. The surface unit cell was taken as a 6×4 lattice, where two Cr atoms can be placed at $2a$ without interaction between dimers. The k-point sampling was $1 \times 3 \times 1$. The structures were relaxed until forces were smaller than 0.01 eV/\AA for the three topmost layers and the Cr structures.

* These authors contributed equally

† nicolas.lorente@ehu.eus

‡ heinrich.andreas@qns.science

§ djchoi@dipc.org

- [1] J. Kim, W.-J. Jang, T. H. Bui, D.-J. Choi, C. Wolf, F. Delgado, D. Krylov, S. Lee, S. Yoon, C. P. Lutz, A. J. Heinrich, and Y. Bae, "Spin resonance amplitude and frequency of a single atom on a surface in a vector magnetic field," (2021), arXiv:2103.09582 [cond-mat.mes-hall].
- [2] C. Mier, B. Verlhac, L. Garnier, R. Robles, L. Limot, N. Lorente, and D.-J. Choi, The Journal of Physical Chemistry Letters **12**, 2983 (2021), <https://doi.org/10.1021/acs.jpcclett.1c00328>.
- [3] M. Ruby *et al.*, Phys. Rev. Lett. **115**, 087001 (2015).
- [4] D.-J. Choi, C. Rubio-Verdú, J. de Bruijckere, M. M. Ugeda, N. Lorente, and J. I. Pascual, Nature Communications **8**, 15175 (2017).
- [5] G. Kresse and J. Furthmüller, Computational Materials Science **6**, 15 (1996).

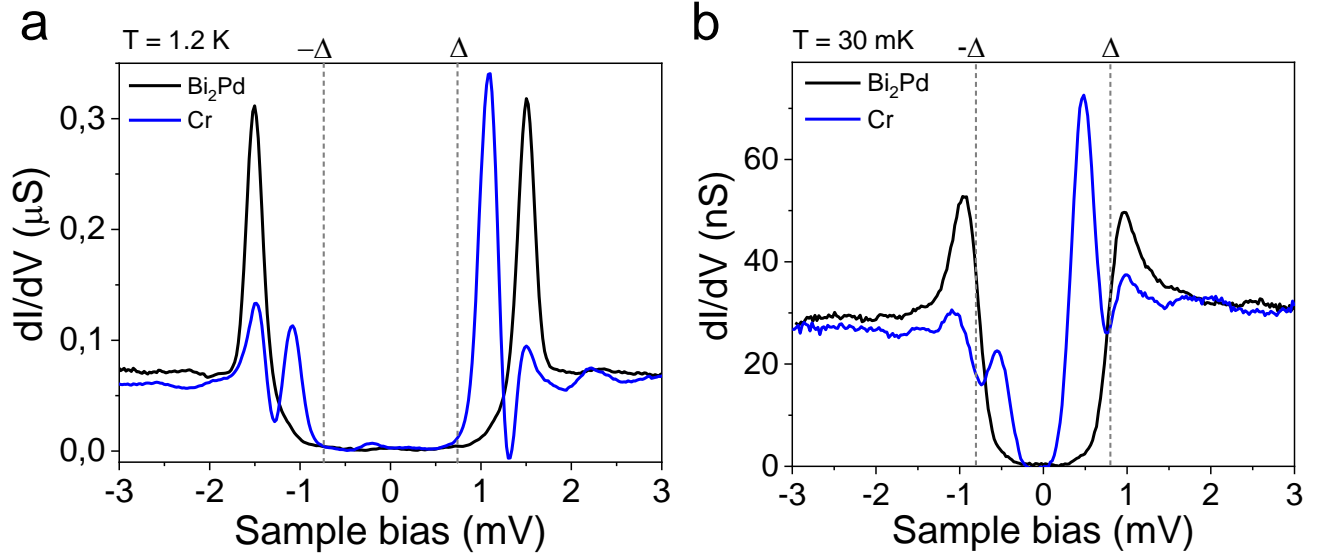


FIG. 1. Comparison of the differential conductance measured on a single Cr atom (blue curve) and on a bare β -Bi₂Pd surface (black curve) with superconducting and non-superconducting tips. The dI/dV spectra using (a) a superconducting (coated with Bi₂Pd) tip at $T = 1.2$ K (adapted from Ref. 6) and (b) a normal metallic PtIr tip at $T = 30$ mK.

[6] D.-J. Choi, C. G. Fernández, E. Herrera, C. Rubio-Verdú, M. M. Ugeda, I. Guillamón, H. Suderow, J. I. Pascual, and N. Lorente, *Phys. Rev. Lett.* **120**, 167001 (2018).

[7] J. P. Perdew, K. Burke, and M. Ernzerhof, *Physical Review Letters* **77**, 3865 (1996).

[8] E. Herrera, I. Guillamón, J. A. Galvis, A. Correa, A. Fente, R. F. Lucas, F. J. Mompean, M. Garcia-Hernandez, S. Vieira, J. P. Brison, and H. Suderow, *Physical Review B* **92**, 054507 (2015).

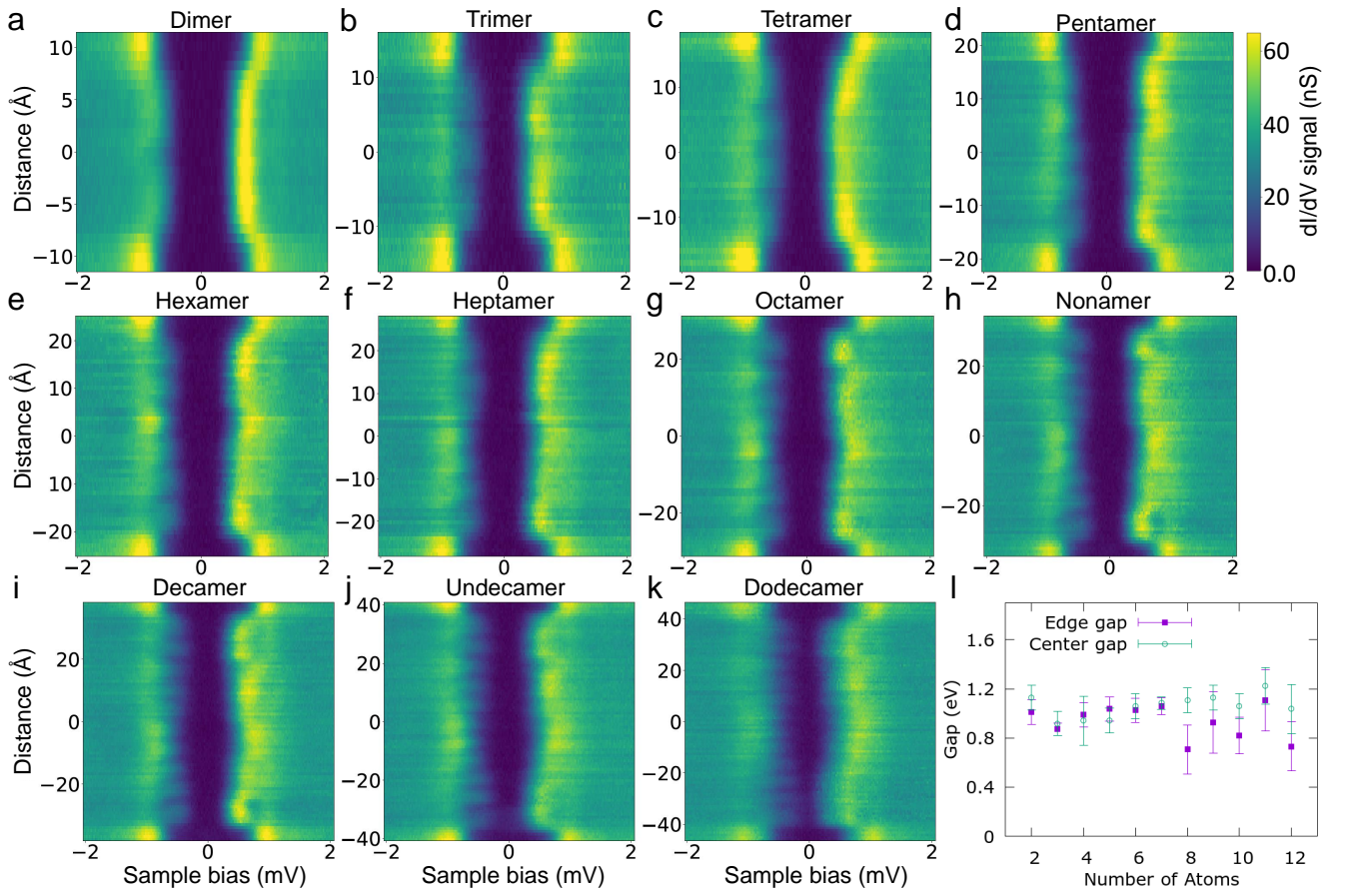


FIG. 2. Differential conductance measured along for $\text{Cr}_n 2a - \langle 100 \rangle$ chains with $n = 2 \dots 12$. Figure 2 of the main text reproduces some of the panels of this figure. The gap has been obtained at an edge atom or at the center of the spin chain. In both cases the gaps are constant within the experimental error.